Dalton Transactions

ROYAL SOCIETY OF CHEMISTRY

PAPER

View Article Online
View Journal | View Issue

Cite this: *Dalton Trans.*, 2025, **54**, 12824

Construction of 2,2′:6′,2″-terpyridine-modified porous organic polymers *via* building unit engineering: preferred and universal transition metal carrier and catalytic application

Zhengguang Li,[a] Yaqin Li,[a] Yongxin Liu,[a] Kaixiu Li,[a] Fan Fu,[a] Mingliang Liu,[a] Jie Yuan,[c] Tao Zhang,[a] Jun Wang,[b] Yiming Li,[a] Fenghua Shen,[d] Hui Liu,[d] Pingshan Wang *[a,b] and Die Liu *[a]

Porous organic polymers (POPs) serve a key function as transition metal carriers and have attracted widespread attention in the catalysis field. However, a preferred and universal transition metal carrier remains elusive. In this study, we designed and synthesized a preferred 2,2′:6′,2″-terpyridine-containing building motif and prepared a POP (**POP-Tpy-1**) *via* the Buchwald–Hartwig coupling reaction of a diamino-linker and trisbromo-node. Taking full advantage of the strong bonding ability of the terpyridine moiety and the availability of binding room, coupled with the high stability of the POP itself, **POP-Tpy-1** displayed universal coordination binding and a high load capacity for many common transition metals (Mn^{2+}, Fe^{3+}, Co^{2+}, Ni^{2+}, Cu^{2+}, Zn^{2+}, Ru^{3+}, Pd^{2+}, Fe^{2+}, and Cu^{+}). The corresponding metal-loaded porous organic polymers (**POP-Tpy-1-M**) can serve as transition metal heterogeneous catalysts, and these were conceptually verified by typical synthesis reactions, including cross-dehydrogenative coupling, click reactions, and Suzuki–Miyaura coupling reactions.

Received 26th June 2025,
Accepted 1st August 2025

DOI: 10.1039/d5dt01504a

rsc.li/dalton

Introduction

Porous organic polymers (POPs), such as conjugated microporous polymers (CMPs),[1–3] porous aromatic frameworks (PAFs),[4,5] and covalent organic frameworks (COFs),[6] have always attracted the attention of researchers because of their unique properties, which include enhanced stability,[7] large specific surface area,[8,9] adjustable pore sizes,[10] accessible modifications,[11–14] and excellent adsorption capacity.[15,16] Because of these properties, POPs can serve as carriers for prepared heterogeneous transition-metal catalysts.[17–19] The general methods for introducing metal ions into POPs involve coordination reactions, including pre- and post-synthetic routes.[20] By comparison, the post-synthetic metalation method is more readily accessible because mixing POP supports with metal precursors is facile.[21,22] Additionally, metal loading can be adjusted by controlling the ratio of the metal species to the bonding sites.[23] Previous reports indicate that post-synthetic metalated POPs were easily obtained by embedding metal species as nanoparticles.[24] However, such loading requires large POP pore sizes and increases synthesis difficulties. In comparison, metalation *via* coordination remains the prevailing method for preparing dispersed heterogeneous catalysts.[25–27] A series of heterogeneous transition metal catalysts have been prepared *via* coordination-reduced metalation of porous materials from N, P, and O atoms containing building blocks with inherent single-pair electrons, such as pyridines,[20] imines,[28–31] phosphine ligands,[32,33] bidentate amine ligands,[34–39] and other compounds.[40–45] However, these monodentate and bidentate ligands can only coordinate with specific transition metals. In comparison, N,N,N-tridentate ligands possess stronger coordination ability and have been appropriately introduced into polymer skeleton structures to construct high-performance single-atom catalysts.[46,47] Meanwhile, triamine unit-embedded polymers have a universal loading capacity for most common transition metals.[48] It is also worth noting that the POPs capable of simultaneously loading bimetals or multi-metals are of great importance in

[a]*Department of Organic and Polymer Chemistry; Hunan Key Laboratory of Micro & Nano Materials Interface Science, College of Chemistry and Chemical Engineering; Central South University, Changsha, Hunan-410083, China.*
E-mail: chemwps@csu.edu.cn, chem-ld@csu.edu.cn
[b]*Institute of Environmental Research at Greater Bay Area; Key Laboratory for Water Quality and Conservation of the Pearl River Delta, Ministry of Education; Guangzhou Key Laboratory for Clean Energy and Materials, Guangzhou University, Guangzhou, Guangdong-510006, China*
[c]*School of Chemistry and Chemical Engineering, Henan Normal University, Xinxiang, Henan 453007, China*
[d]*School of Metallurgy and Environment, Central South University, Changsha, Hunan-410083, China*

order to achieve a cascade catalytic reaction, thus improving synthesis efficiency.[49–51] 2,2′:6′,2″-Terpyridine (tpy) compounds are appealing tridentate pincer ligands and display tight chelation with various transition metals. Moreover, their transition metal complexes have been widely used in homogeneous catalysis.[52] Recently, Jiang *et al.* reported anchoring Pt^{2+} cations by introducing a tpy unit at the edge of a one-dimensional (1D) COF, which exhibited high photocatalytic activity for hydrogen evolution from water.[53] Yam *et al.* synthesized two robust nitrogen-rich COFs *via* a "bottom-up" pore-wall-bearing terpyridine unit strategy, which exhibited excellent removal efficiency and capacity for a variety of heavy metal ions in water.[48] Unfortunately, tpy-containing polymers bear a coplanar conformation between the tpy moiety and the linker and are prone to form π–π stacking.[54] Such compact stacking reduces the accessibility of tpy to metal ions due to the pseudo-octahedral coordination configuration of most of the tpy transition metal complexes. We argue that the introduction of steric hindrance between the tpy moiety and the linker of the structural motif reduces the planarity, which would endow the tpy moiety with sufficient space to bind metal ions after polymerization. Therefore, in this study, diamino units bent to 120° with an inwardly or outwardly oriented tpy moiety were designed and synthesized. Subsequently, two novel POPs containing an inward tpy anchor (**POP-Tpy-1**, Fig. 1) or outward tpy anchor (**POP-Tpy-2**) were prepared *via* Buchwald–Hartwig (B–H) coupling. As expected, **POP-Tpy-1** displayed a better load capacity than **POP-Tpy-2**. Meanwhile, **POP-Tpy-1** showed universality for transition metal loading, and a series of metalized POPs (**POP-Tpy-1-M**) were prepared by simply mixing **POP-Tpy-1** with transition metal salts. Furthermore, the application of these metal-loaded polymers as catalysts for Suzuki coupling, click reactions, and cross-dehydrogenative coupling (CDC) was explored.

Results and discussion

As shown in Scheme 1, building block **L1** was designed as a compact structure with two 4-aminophenyl groups located

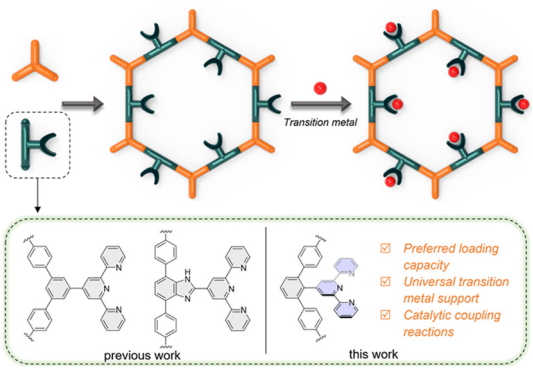

Fig. 1 Schematic illustration of the preparation of the tpy-containing porous organic polymer and subsequent metal loading *via* post-synthetic routes.

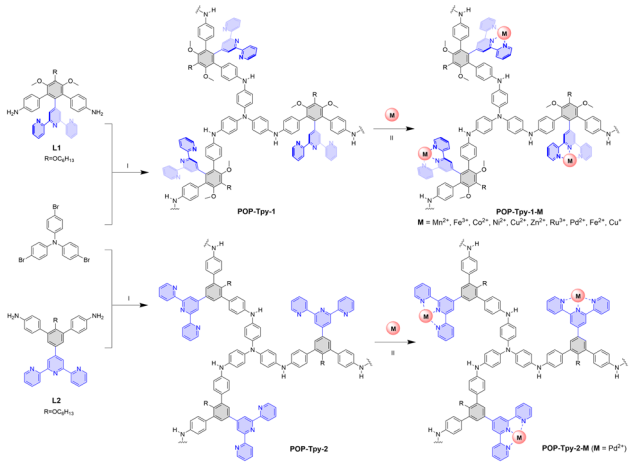

Scheme 1 Synthetic route of **POP-Tpy-1/2** and **POP-Tpy-1/2-M** (reagents and conditions: (I) $Pd(dba)_2$, XPhos, NaO*t*Bu, THF, 65 °C, 48 h; (II) MeOH or CH_2Cl_2/CH_3CN, metal salt).

adjacent to the tpy moiety to form a ligand with non-planar geometry. For comparison, the stretched **L2** contains an outwardly oriented tpy moiety. The structures of **L1** and **L2** were characterized by nuclear magnetic resonance (NMR) spectroscopy, including ^1H, ^{13}C, 2D COSY, and 2D NOESY, and electrospray ionization mass spectrometry (ESI-MS) (Fig. S1–S17). Two POPs, **POP-Tpy-1** and **POP-Tpy-2**, were prepared using the B–H coupling reaction of ligands **L1**/**L2** and tris(4-bromophenyl)amine, respectively. The specific synthetic route is shown in Scheme S1. The chemical compositions and structures of **POP-Tpy-1/2** were initially confirmed by Fourier transform infrared (FT-IR) spectroscopy and powder X-ray diffraction (PXRD). The bands of the primary amine group of **L1** at 3449 and 3363 cm^{-1} ($-NH_2$ stretching), and those of the aromatic C–Br groups of tris(4-bromophenylamine) at 1179 cm^{-1} (aromatic C–Br stretching), were absent in the spectrum of **POP-Tpy-1**. A series of distinct signal peaks at 2933, 1599, 1498, 1452, and 808 cm^{-1} originating from C–H stretching, and C–N, C–C, C=N, and aryl C–H deformation of **POP-Tpy-1** were observed, further suggesting the formation of polymers (Fig. 2a).

Similarly, the structure of **POP-Tpy-2** was fully characterized (Fig. S34a, S36). The PXRD patterns of **POP-Tpy-1** and **POP-Tpy-2** showed highly broad diffraction peaks at 2θ = ~18–20°, indicating their amorphous structure. The porosity of **POP-Tpy-1/2** was analyzed by measuring their nitrogen adsorption/desorption isotherms (Fig. 2b). According to the calculations, the Brunauer–Emmett–Teller (BET) surface area of **POP-Tpy-1** was 190 $m^2\ g^{-1}$, while the BET value for **POP-Tpy-2** was only 2 $m^2\ g^{-1}$. This occurrence served as preliminary verification of our previous hypothesis that **POP-Tpy-2** displays tighter stacking, resulting in a decreased surface area.

To validate our conjecture about conformational differences, single-crystal structures of **L1′** (CH_3O- instead of $nC_6H_{13}O-$ of **L1**) and **L2** were analyzed. The tpy moiety and the linked benzene in **L2** were nearly coplanar and their dihedral angles were 12.298° and 12.120°, respectively, corresponding

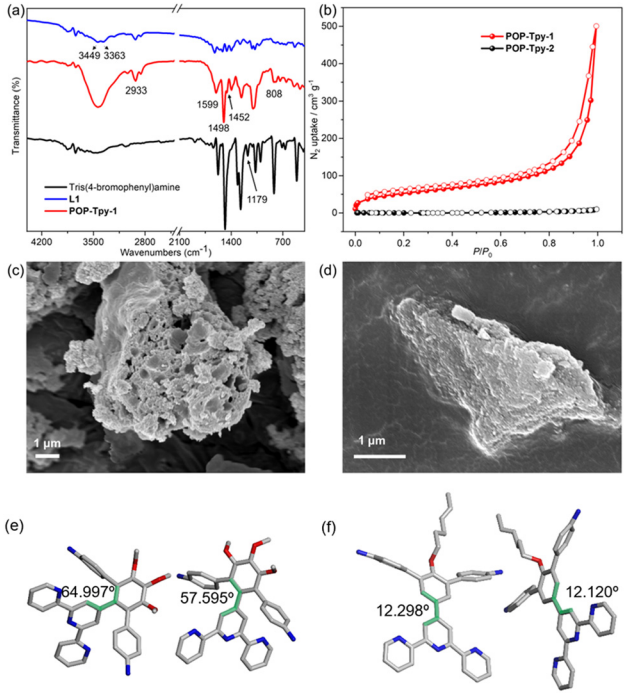

Fig. 2 (a) FT-IR spectra of tris(4-bromophenyl)amine, **L1**, and **POP-Tpy-1**. (b) N_2 adsorption/desorption isotherms, and (c and d) SEM images of **POP-Tpy-1** and **POP-Tpy-2**. (e and f) Single-crystal structures of **L1′** and **L2**.

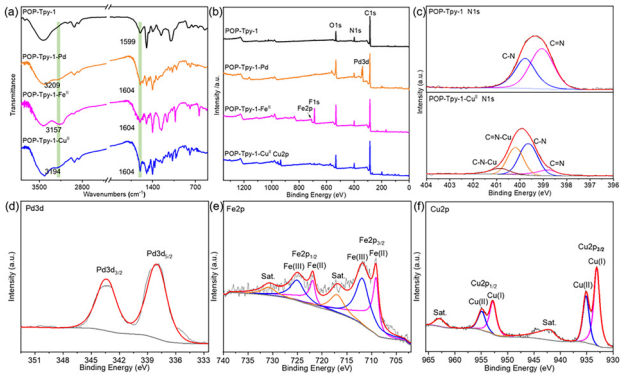

Fig. 3 (a) Fourier transform infrared spectra of **POP-Tpy-1-M**, (b) XPS spectra of **POP-Tpy-1-M**, (c) N 1s core-level XPS spectra of **POP-Tpy-1**/**POP-Tpy-1-Cu^{II}**, and (d)–(f) Pd 3d, Fe 2p, and Cu 2p core-level XPS spectra of **POP-Tpy-1-Pd/Fe^{II}/Cu**.

to those of the two conformations in single crystals. In sharp contrast, the angles for **L1′** were obviously larger (64.997° and 57.595°) (Fig. 2e, f, and S68, S69). The single-crystal structure analysis fully supports the conformational differences of **L1** and **L2**. Furthermore, the thermal and chemical stabilities of **POP-Tpy-1/2** were evaluated using thermogravimetric analysis (TGA). Both **POP-Tpy-1** and **POP-Tpy-2** displayed high thermal stability; the decomposition temperatures were 405 and 439 °C, respectively, which can be attributed to the crosslinked rigid aromatic structures (Fig. S35). The morphologies of **POP-Tpy-1** and **POP-Tpy-2** were observed from their scanning electron microscopy (SEM) and transmission electron microscopy (TEM) profiles. The SEM and TEM images showed that **POP-Tpy-1/2** consisted of aggregated nanoparticles (Fig. 2c, d, 4a, and S51). The N 1s spectrum of **POP-Tpy-1** displayed two individual peaks at 399.0 and 399.7 eV, which were assigned to the signals of the C=N bond of pyridine and the C–N bond of the aniline moiety, respectively (Fig. 3c).[55] The tpy moiety, which contains three nitrogen atoms, exhibits a preferred coordination performance toward transition metal ions, forming mono-tpy pincer complexes.[56] Therefore, **POP-Tpy-1/2** structures were further assessed as carriers for common transition metals *via* metalation. **POP-Tpy-1/2-M** complexes were prepared by simply mixing **POP-Tpy-1/2** with different metal salts ($MnCl_2$, $FeCl_3$, $CoCl_2{\cdot}6H_2O$, $NiCl_2{\cdot}H_2O$, $CuCl_2{\cdot}2H_2O$, $ZnCl_2$, $RuCl_3{\cdot}6H_2O$, $PdCl_2$, $Fe(OTf)_2$, and $Cu(CH_3CN)_4BF_4$ for **POP-Tpy-1** and $PdCl_2$ for **POP-Tpy-2**), respectively. The SEM images show that **POP-Tpy-1-M** (**M** = Mn^{2+}, Fe^{3+}, Co^{2+}, Ni^{2+}, Cu^{2+}, Zn^{2+}, Ru^{3+}, Pd^{2+}, Fe^{2+}, and Cu^{+}) comprised aggregated nanoparticles similar to **POP-Tpy-1**. No evident morphological changes were observed before or after coordination (Fig. S38–S50), demonstrating the structural stability of **POP-Tpy-1**.

Furthermore, the composition of the metallo-polymers was characterized by SEM energy-dispersive X-ray spectroscopy (EDX) elemental mapping, in which the elemental distributions including those of non-metallic (C, N, O, and Cl) and metallic elements (Mn, Fe, Co, Ni, Cu, Zn, Ru, and Pd) were observed (Fig. S38–S50). The XPS spectra further confirmed the presence of C, N, Cl, Mn, Fe, Co, Ni, Cu, Zn, Ru, and Pd in **POP-Tpy-1-M** (Fig. S54–S63). The Cu 2p core-level XPS spectrum peaks of **POP-Tpy-1-Cu^{II}** at 935.1/954.9 eV and 933.1/952.7 eV correspond to Cu^{2+} and Cu^{+}, respectively (Fig. 3f). The Pd 3d core-level XPS spectrum showed two broad peaks at 337.2 and 342.5 eV (Fig. 3d).[57] Based on the N 1s spectrum, C=N–Cu, C=N–Pd, and C=N–Fe bonds are evidently predominant in **POP-Tpy-1-Cu^{II}**, **POP-Tpy-1-Pd** and **POP-Tpy-1-Fe^{II}**, respectively, confirming the coordination between the tpy moiety and the metal ions (Fig. 3c, S64b and S64c). However, it is undeniable that there are still free tpy moieties after metalation, possibly due to no ion diffusion channels resulting from compact stacking. Additionally, from the FT-IR spectra of **POP-Tpy-1-Pd**, **POP-Tpy-1-Fe^{II}**, and **POP-Tpy-1-Cu^{II}**, noticeable changes were observed, *e.g.*, the vibrational mode at 1599 cm^{-1} partially shifts to 1604 cm^{-1}, further supporting successful binding of the pyridine N atoms of tpy to metal ions (Fig. 3a).

TEM was widely used to characterize the distribution of transition metals in **POP-Tpy-1-M**. As shown in Fig. 4, the TEM profiles of **POP-Tpy-1-M** were markedly different from those of **POP-Tpy-1**. **POP-Tpy-1** displayed a low contrast, indicative of a non-metallic component, whereas **POP-Tpy-1-M** displayed a noticeably higher contrast and uniform distribution, further supporting the introduction of metal elements. The compositional distribution of **POP-Tpy-1-M** was investigated by TEM-EDX elemental mapping, which revealed an overlay of C,

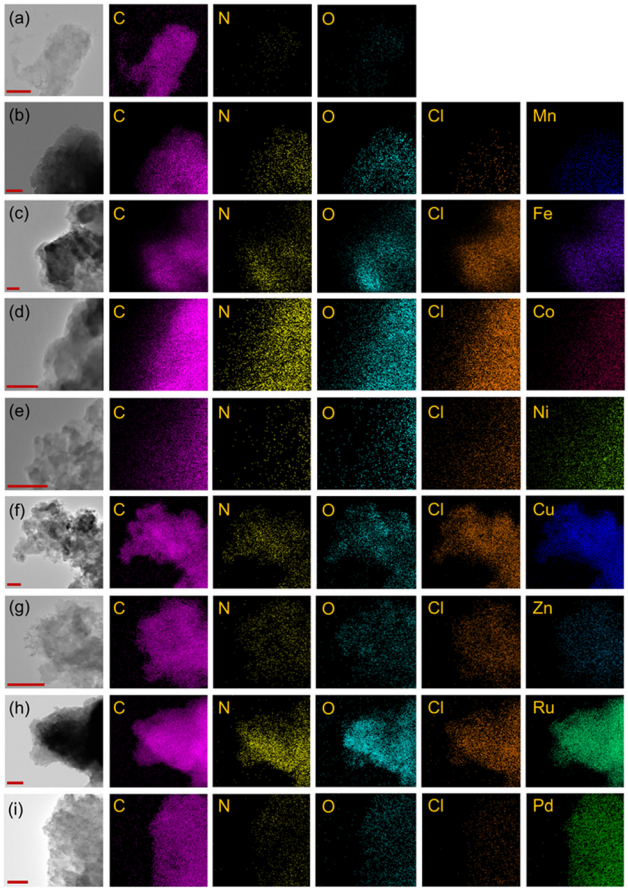

Fig. 4 TEM images of (a) **POP-Tpy-1**, (b) **POP-Tpy-1-Mn**, (c) **POP-Tpy-1-Fe^{III}**, (d) **POP-Tpy-1-Co**, (e) **POP-Tpy-1-Ni**, (f) **POP-Tpy-1-Cu^{II}**, (g) **POP-Tpy-1-Zn**, (h) **POP-Tpy-1-Ru**, and (i) **POP-Tpy-1-Pd**. Scale bar: 250 nm.

N, O, Cl, and metal ions with clear separation (Fig. 4a–i), particularly for the metal elements.

These results further support the uniform distribution of metal species over the POP structure, indicating that **POP-Tpy-1** can be used as a universal metal carrier to obtain dispersed transition metal catalysts. The metal content of **POP-Tpy-1/2-M** was further determined by inductively coupled plasma optical emission spectrometry (ICP-OES). The theoretical (calculated from the tpy moiety) and experimental contents of each metal species are listed in Table 1.

In sharp contrast, the adsorption capacity of **POP-Tpy-2** for Pd species is significantly lower than that of **POP-Tpy-1**, indicating that **POP-Tpy-1** has more active adsorption sites, further highlighting the importance of the structural design. According to the results above, there are still some uncoordinated terpyridine molecules, consistent with the XPS analysis. The metal content in **POP-Tpy-1-Pd** was the highest among the POPs, nearly at 100% of the theoretical capacity, which could be attributed to the fact that a portion of the metal ions was embedded between the layers *via* complexation with the nitrogen atoms of the aniline groups.[29] Meanwhile, high-angle

Table 1 Metal loading contents of **POP-Tpy-1/2-M**

Entry	Catalyst	Theoretical content[a] (%)	ICP-OES (wt%)
1	**POP-Tpy-1-Mn**	6.41	2.33
2	**POP-Tpy-1-Fe^{III}**	6.26	3.17
3	**POP-Tpy-1-Co**	6.85	3.15
4	**POP-Tpy-1-Ni**	6.82	2.91
5	**POP-Tpy-1-Cu^{II}**	7.35	3.06/1.76[b]
6	**POP-Tpy-1-Zn**	7.54	5.03
7	**POP-Tpy-1-Ru**	10.78	1.56
8	**POP-Tpy-1-Pd**	11.72	11.37/4.36[b]
9	**POP-Tpy-1-Fe^{II}**	5.15	2.70/1.03[b]
10	**POP-Tpy-1-Cu^{I}**	7.21	2.03
11	**POP-Tpy-2-Pd**	12.55	6.35
12	**POP-Tpy-1-Cu^{I}/Pd** 4 : 1	—	Cu: 1.84 Pd: 0.50
13	**POP-Tpy-1-Cu^{I}/Pd** 1 : 1	—	Cu: 1.11 Pd: 0.85
14	**POP-Tpy-1-Cu^{I}/Pd** 1 : 2	—	Cu: 0.64 Pd: 1.20

[a] Calculated based on the tpy monomer. [b] Metal loading content after five cycling experiments.

annular dark-field scanning transmission electron microscopy (HAADF-STEM) images showed the presence of single-atom-dispersed and clustered Pd species in **POP-Tpy-1-Pd** (Fig. 5). We speculate that the formation of nanoclusters was stabilized by nitrogen ligand protection and cavity confinement.[58,59] In addition, the specific surface area of three catalysts **POP-Tpy-1-Cu^{II}/Pd/Fe^{II}** decreased significantly after metalation, with values of 20, 16, and 17 $m^2\ g^{-1}$, respectively (Fig. S37).

To validate the catalytic ability of metal-loaded POPs, the catalytic performance of **POP-Tpy-1-Cu^{II}** in a click reaction was first evaluated. As shown in Table 2, cycloaddition between azides and alkynes was performed using **POP-Tpy-1-Cu^{II}** as the catalyst. The yields of the reaction products (**8a–8e**) all exceeded 90%, using the different alkyne-based substrates. The yield of **8a** still remained above 90% after five cycles of the reaction (Fig. S65). The catalytic activity of **POP-Tpy-1-Pd** in a Pd-catalyzed Suzuki–Miyaura coupling reaction was also examined. The substituted aryl bromides afforded cross-coupling products (**9a–9d**) in excellent isolated yields (84–93%). These results indicate that **POP-Tpy-1-Pd** exhibits high catalytic activity in Suzuki–Miyaura coupling reactions.

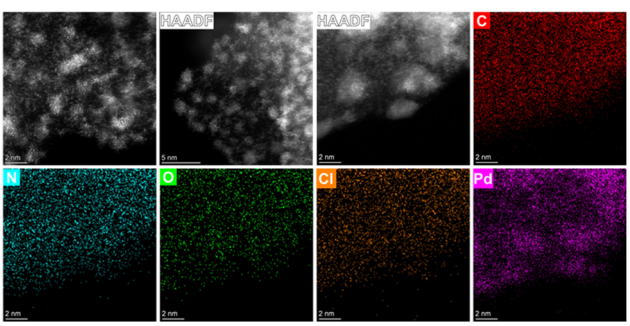

Fig. 5 HAADF-STEM images and the corresponding elemental mapping of **POP-Tpy-1-Pd**.

Table 2 Optimization experiments of the click and Suzuki–Miyaura coupling reactions

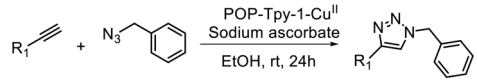

Entry	R_1	Product	Yield (%)
1		**8a**	93
2		**8b**	94
3	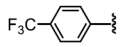	**8c**	90
4	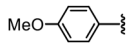	**8d**	95
5	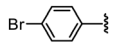	**8e**	93

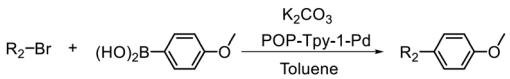

Entry	R_2	Product	Yield (%)
6	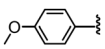	**9a**	91
7	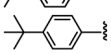	**9b**	86
8	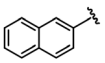	**9c**	84
9	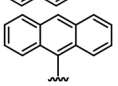	**9d**	93

In contrast, when **POP-Tpy-2-Pd** was used as the catalyst for the preparation of compound **9b**, an isolated yield of only 56% was obtained. This is mainly because **POP-Tpy-2-Pd** is more densely packed, resulting in a lower content of Pd metal (Table 1), once again proving the rationality of the mentioned ligand design with increased steric hindrance. The **POP-Tpy-1-Pd** catalyst was readily recycled *via* facile filtration and solvent washing. When aryl bromide and methoxyphenylboronic acid were used as substrates, the recyclability tests showed that the yield of the cross-coupling product remained at 52% after five repeated reactions with the recycled catalysts (Fig. S66). A significant drop in product yield following the first catalyst recycling can be attributed to the re-addition of K_2CO_3, which leads to the dissociation of metals from the POP. After catalytic cycling, we retested the BET surface areas of catalysts, which were determined to be 11 $m^2\ g^{-1}$ for **POP-Tpy-1-Cu^{II}** and 22 $m^2\ g^{-1}$ for **POP-Tpy-1-Pd** (Fig. S37b). The results indicate that they still maintained their porous structure, supporting the structural stability of the catalysts.

To verify the universality of **POP-Tpy-1-M** as a metal catalyst, CDC reactions were conducted using **POP-Tpy-1-Fe^{II}** as the catalyst (Fig. 6). After separation by column chromatography, the highest yield of the corresponding oxidative coupling product was 57% (Table S1), and this yield remained above 45% after three consecutive experiments (Fig. S67). Notably, the decrease in catalytic performance of **POP-Tpy-1-Cu^{II}** or **Pd** or **Fe^{II}** can be attributed to the loss of metals; this hypothesis is supported by the reduction in the metal content to 1.76%, 4.36%, and 1.03%, respectively, after five cycles of experiments (Table 1).

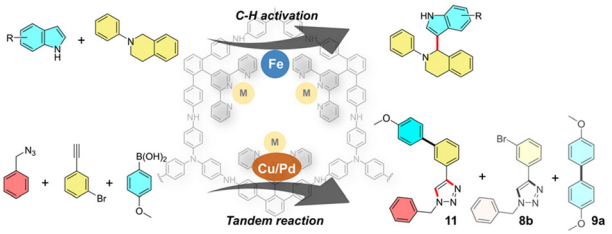

Fig. 6 Diagram of the cross-dehydrogenative coupling reactions catalysed by **POP-Tpy-1-Fe** and the bimetallic catalytic tandem reaction catalysed by **POP-Tpy-1-Cu^{I}/Pd**.

Furthermore, three bimetallic catalysts, **POP-Tpy-1-Cu^{I}/Pd**, were synthesized by mixing **POP-Tpy-1** with different ratios of $Cu(CH_3CN)_4BF_4$ and $PdCl_2$ (4/1, 1/1 and 1/2), demonstrating universal multi-metal load capacity. The composition of the bimetallic catalyst **POP-Tpy-1-Cu^{I}/Pd** was confirmed by ICP-OES and EDX (Table 1 and Fig. S46–S48), in which the Cu and Pd contents were detected, and their ratio was calculated to be 1.84/0.5, 1.11/0.85, and 0.64/1.2 wt%, respectively. Notably, the ratio of the actual metal content of Cu and Pd was consistent with the initial added ratio of the metal, supporting the controllability of metal loading. **POP-Tpy-1-Cu^{I}/Pd** catalysts were used to catalyze the tandem reaction (Fig. 6). Interestingly, only **POP-Tpy-1-Cu$_{1.11}$/Pd$_{0.85}$** could catalyze the substrates to form the target product **11** with a yield of 20%. Both **POP-Tpy-1-Cu$_{1.84}$/Pd$_{0.5}$** and **POP-Tpy-1-Cu$_{0.64}$/Pd$_{1.12}$** afforded the desired products in low yields; the click product **8b** and the self-coupling product **9a** were obtained as the main components in yields of 84%/10% and 16%/18%, respectively (Table S2 and Fig. S31–S33). This result could probably be attributed to the fact that when the Cu content increased, the click reaction became favored and the yield of intermediate **8b** increased; yet, further Suzuki coupling occurred with difficulty, and the yield of product **11** decreased. When the Cu content decreased and the Pd content increased, the amount of intermediate, **8b**, decreased, and complicated products were formed *via* the Sonogashira coupling reaction of the alkynyl compound, Suzuki coupling, and self-coupling of boric acid. These results provide a new avenue for controlling cascade reactions using multi-metal-loaded POPs.

Conclusions

In conclusion, a novel tpy-modified POP was designed and prepared *via* B–H coupling between a tpy-containing unit and tris(4-bromophenyl)amine. Given its universal coordination tendency toward transition-metal ions, metal–organic composites can be easily obtained by mixing the POP with the most common transition metals, including Mn^{2+}, Fe^{3+}, Co^{2+}, Ni^{2+},

Cu^{2+}, Zn^{2+}, Ru^{3+}, Pd^{2+}, Fe^{2+}, and Cu^{+}. Notably, an increase in the metal loading capacity was achieved by manipulating the geometry of the building blocks to reduce stacking and increase the binding space; this is particularly significant for future design of metal adsorption materials. Furthermore, POPs as catalysts displayed universal catalytic behavior and excellent performance in the click reaction, Suzuki–Miyaura coupling, and CDC. This study provides a new and superior POP for use as a versatile transition metal carrier. In the future, such tpy-modified POPs may be used for the extraction and separation of metal ions from wastewater, and as powerful catalysts to achieve highly efficient photocatalytic and electrocatalytic performances.

Author contributions

Z. G. L., investigation, formal analysis, writing – original draft, and funding acquisition; also prepared the samples and performed general characterization of the compounds. Y. Q. L., Y. X. L., K. X. L., F. F., and M. L. L., data curation and investigation: prepared the samples, performed general characterization of the compounds, and analysed the ^{1}H NMR data. J. Y. and J. W., investigation and formal analysis: acquired and analysed the ESI-MS data. T. Z., Y. M. L. and F. H. S., investigation and resources: performed SEM and ICP-OES and analysed the data. H. L., P. S. W. and D. L., conceptualization, formal analysis, resources, funding acquisition, supervision, and writing – review & editing.

Conflicts of interest

There are no conflicts to declare.

Data availability

The data that support the findings of this study are available in the main text and the SI.

The supporting data is presented in the SI: Experimental procedures and characterization data, including ^{1}H, ^{13}C, COSY, NOESY NMR spectra of the new compounds, PXRD, FT-IR, TGA, ESI-MS spectra, TEM, SEM of related compounds. See DOI: **https://doi.org/10.1039/d5dt01504a**.

CCDC 2403377 and 2403378 contain the supplementary crystallographic data for this paper.[60a,b]

Acknowledgements

We acknowledge the support from the Major Science and Technology Projects of Yunnan Province (No: 202302AB080016), the National Natural Science Foundation of China (No: 22001047 for D. L. and No: 21971257 for P. S. W.), and the Fundamental Research Funds for the Central Universities of Central South University (No: 2023ZZTS0437 for Z. G. L.). The authors gratefully acknowledge the Center for Advanced Research at CSU for the NMR measurements.

References

1 A. I. Cooper, *Adv. Mater.*, 2009, **21**, 1291–1295.
2 R. Dawson, A. I. Cooper and D. J. Adams, *Prog. Polym. Sci.*, 2012, **37**, 530–563.
3 J. Tan, W.-J. Chen and J. Guo, *Chin. Chem. Lett.*, 2016, **27**, 1405–1411.
4 T. Ben and S. Qiu, *CrystEngComm*, 2013, **15**, 17–26.
5 T. Ben, H. Ren, S. Ma, D. Cao, J. Lan, X. Jing, W. Wang, J. Xu, F. Deng, J. M. Simmons, S. Qiu and G. Zhu, *Angew. Chem., Int. Ed.*, 2009, **48**, 9457–9460.
6 A. P. Côté, A. I. Benin, N. W. Ockwig, M. O'Keeffe, A. J. Matzger and O. M. Yaghi, *Science*, 2005, **310**, 1166–1170.
7 R. Liu, K. T. Tan, Y. Gong, Y. Chen, Z. Li, S. Xie, T. He, Z. Lu, H. Yang and D. Jiang, *Chem. Soc. Rev.*, 2021, **50**, 120–242.
8 H. Li, J. Chang, S. Li, X. Guan, D. Li, C. Li, L. Tang, M. Xue, Y. Yan, V. Valtchev, S. Qiu and Q. Fang, *J. Am. Chem. Soc.*, 2019, **141**, 13324–13329.
9 N. Huang, P. Wang and D. Jiang, *Nat. Rev. Mater.*, 2016, **1**, 16068.
10 Y. Xia, W. Zhang, S. Yang, L. Wang and G. Yu, *Adv. Mater.*, 2023, **35**, 2301190.
11 Y. Deng, Z. Zhang, P. Du, X. Ning, Y. Wang, D. Zhang, J. Liu, S. Zhang and X. Lu, *Angew. Chem., Int. Ed.*, 2020, **59**, 6082–6089.
12 Q. Liao, C. Ke, X. Huang, D. Wang, Q. Han, Y. Zhang, Y. Zhang and K. Xi, *Angew. Chem., Int. Ed.*, 2020, **60**, 1411–1416.
13 C. Yuan, X. Wu, R. Gao, X. Han, Y. Liu, Y. Long and Y. Cui, *J. Am. Chem. Soc.*, 2019, **141**, 20187–20197.
14 Y. Yan, X. Li, G. Chen, K. Zhang, X. Tang, S. Zhang, S. Zheng, J. Fan, W. Zhang and S. Cai, *Chin. Chem. Lett.*, 2021, **32**, 107–112.
15 Q. Hao, Y. Tao, X. Ding, Y. Yang, J. Feng, R.-L. Wang, X.-M. Chen, G.-L. Chen, X. Li, H. OuYang, X. Hu, J. Tian, B.-H. Han, G. Zhu, W. Wang, F. Zhang, B. Tan, Z.-T. Li, D. Wang and L.-J. Wan, *Sci. China: Chem.*, 2023, **66**, 620–682.
16 A. K. Sekizkardes, P. Wang, J. Hoffman, S. Budhathoki and D. Hopkinson, *Mater. Adv.*, 2022, **3**, 6668–6686.
17 S. Kramer, N. R. Bennedsen and S. Kegnæs, *ACS Catal.*, 2018, **8**, 6961–6982.
18 R. Tao, X. Ma, X. Wei, Y. Jin, L. Qiu and W. Zhang, *J. Mater. Chem. A*, 2020, **8**, 17360–17391.
19 Y. Yang, Y. Xiao, L. Jiang, J. Li, J. Li, J. Jia, C. T. Yavuz, F. Cui, X. Jing and G. Zhu, *Adv. Mater.*, 2024, **36**, 2404791.
20 J. X. Jiang, C. Wang, A. Laybourn, T. Hasell, R. Clowes, Y. Z. Khimyak, J. Xiao, S. J. Higgins, D. J. Adams and A. I. Cooper, *Angew. Chem., Int. Ed.*, 2011, **50**, 1072–1075.

21 R. Luo, M. Chen, X. Liu, W. Xu, J. Li, B. Liu and Y. Fang, *J. Mater. Chem. A*, 2020, **8**, 18408–18424.
22 Z. Li, X. Shi, H. Cheng, Y. Song, Y. Jiao, S. Shi, J. Gao and J. Hou, *Adv. Energy Mater.*, 2024, **14**, 2302797.
23 M. Lv, C.-X. Cui, N. Huang, M. Wu, Q. Wang, T. Gao, Y. Zheng, H. Li, W. Liu, Y. Huang, T. Ma and L. Ye, *Angew. Chem., Int. Ed.*, 2024, **63**, e202315802.
24 S. Lu, Y. Hu, S. Wan, R. McCaffrey, Y. Jin, H. Gu and W. Zhang, *J. Am. Chem. Soc.*, 2017, **139**, 17082–17088.
25 W. M. Bloch, A. Burgun, C. J. Coghlan, R. Lee, M. L. Coote, C. J. Doonan and C. J. Sumby, *Nat. Chem.*, 2014, **6**, 906–912.
26 J. Guo, Q. Xia, W. Y. Tang, Z. Li, X. Wu, L.-J. Liu, W.-P. To, H.-X. Shu, K.-H. Low, P. C. Y. Chow, T. W. B. Lo and J. He, *Nat. Catal.*, 2024, **7**, 307–320.
27 Y. Pi, X. Feng, Y. Song, Z. Xu, Z. Li and W. Lin, *J. Am. Chem. Soc.*, 2020, **142**, 10302–10307.
28 L. Ran, Z. Li, B. Ran, J. Cao, Y. Zhao, T. Shao, Y. Song, M. K. H. Leung, L. Sun and J. Hou, *J. Am. Chem. Soc.*, 2022, **144**, 17097–17109.
29 S.-Y. Ding, J. Gao, Q. Wang, Y. Zhang, W.-G. Song, C.-Y. Su and W. Wang, *J. Am. Chem. Soc.*, 2011, **133**, 19816–19822.
30 C.-T. Kuo, Y. Lu, P. Arab, K. S. Weeraratne, H. El-Kaderi and A. M. Karim, *Cell Rep. Phys. Sci.*, 2021, **2**, 100495.
31 C. Zhu, M. Yang, B. Jiang, L. Lu, Q. Fang, Y. Zheng, S. Song, B. Chen and Y. Shen, *Nat. Commun.*, 2025, **16**, 790.
32 Z. Zheng, C. Yuan, M. Sun, J. Dong, Y. Liu and Y. Cui, *J. Am. Chem. Soc.*, 2023, **145**, 6100–6111.
33 R. Tao, X. Shen, Y. Hu, K. Kang, Y. Zheng, S. Luo, S. Yang, W. Li, S. Lu, Y. Jin, L. Qiu and W. Zhang, *Small*, 2020, **16**, 1906005.
34 Q. Sun, B. Aguila, J. Perman, N. Nguyen and S. Ma, *J. Am. Chem. Soc.*, 2016, **138**, 15790–15796.
35 M. Kou, W. Liu, Y. Wang, J. Huang, Y. Chen, Y. Zhou, Y. Chen, M. Ma, K. Lei, H. Xie, P. K. Wong and L. Ye, *Appl. Catal., B*, 2021, **291**, 120146.
36 Y. Liu, C. Wu, Q. Sun, F. Hu, Q. Pan, J. Sun, Y. Jin, Z. Li, W. Zhang and Y. Zhao, *CCS Chem.*, 2020, **3**, 2418–2427.
37 Q. Xu, J. Han, F. Tian, X. Zhao, J. Rong, J. Zhang, P. She, J.-S. Qin and H. Rao, *J. Am. Chem. Soc.*, 2025, **147**, 10587–10597.
38 B. Zhang, H. Li, Y. Kang, K. Yang, H. Liu, Y. Zhao and S. Qiao, *Adv. Funct. Mater.*, 2025, **35**, 2416958.
39 C. Zhu, C. Gong, D. Cao, L.-L. Ma, D. Liu, L. Zhang, Y. Li, Y. Peng and G. Yuan, *Angew. Chem., Int. Ed.*, 2025, **64**, e202504348.
40 J. Dong, X. Han, Y. Liu, H. Li and Y. Cui, *Angew. Chem., Int. Ed.*, 2020, **59**, 13722–13733.
41 Q. Guan, L.-L. Zhou and Y.-B. Dong, *Chem. Soc. Rev.*, 2022, **51**, 6307–6416.
42 N. B. McKeown, S. Makhseed and P. M. Budd, *Chem. Commun.*, 2002, 2780–2781.
43 L. Pan, M.-Y. Xu, L.-J. Feng, Q. Chen, Y.-J. He and B.-H. Han, *Polym. Chem.*, 2016, **7**, 2299–2307.
44 P. Wang, Y. Dai, Z. Song, Y. Wang, J. Wei, Z. Liu, Y. Ma, F. Yang, J. Qu, S. Liu, Y. Cai, X. Yang, C. M. Li and J. Hu, *Chem. Eng. J.*, 2025, **511**, 162084.
45 Y. Han, M. Zhang, Y.-Q. Zhang and Z.-H. Zhang, *Green Chem.*, 2018, **20**, 4891–4900.
46 Y.-Y. Duan, Y. Zhang, Y.-Z. Cheng, X. Bao, K.-F. Gao, B.-R. Huang, S. Li, H.-m. Bai, Y. Gong, D.-H. Yang, X. Ding, F.-t. Li, Q. Zheng, X. Liu and B.-H. Han, *Appl. Catal., B*, 2025, **368**, 125117.
47 L. Fang, S. Qiu, H. Xu, T. Ye and L. Li, *Adv. Funct. Mater.*, 2025, 2504676.
48 H. Z. Wang, M. H. Y. Chan and V. W. W. Yam, *Small Methods*, 2024, **8**, 2400465.
49 X. Chen, J.-Y. Song, J. Zheng, Y.-M. Wang, J. Luo, P. Weng, B.-C. Cai, X.-C. Lin, G.-H. Ning and D. Li, *J. Am. Chem. Soc.*, 2024, **146**, 19271–19278.
50 W. Shi, Y. Quan, G. Lan, K. Ni, Y. Song, X. Jiang, C. Wang and W. Lin, *J. Am. Chem. Soc.*, 2021, **143**, 16718–16724.
51 F. Yang, J. Wang, Y. Wang, B. Yu, Y. Cao, J. Li, L. Wu, J. Huang and Y.-N. Liu, *Angew. Chem., Int. Ed.*, 2024, **63**, e202318115.
52 G. Chelucci and R. P. Thummel, *Chem. Rev.*, 2002, **102**, 3129–3170.
53 C. Liu, D.-L. Ma, P.-J. Tian, C. Jia, Q.-Y. Qi, G.-F. Jiang and X. Zhao, *J. Mater. Chem. A*, 2024, **12**, 16063–16069.
54 J. Zhang, F. Xue and Z. Wang, *Angew. Chem., Int. Ed.*, 2025, **64**, e202425617.
55 J. Zhang and L. Dai, *Angew. Chem., Int. Ed.*, 2016, **55**, 13296–13300.
56 C. Wei, Y. He, X. Shi and Z. Song, *Coord. Chem. Rev.*, 2019, **385**, 1–19.
57 S. Gao, Y. Huang, M. Cao, T.-f. Liu and R. Cao, *J. Mater. Chem.*, 2011, **21**, 16467–16472.
58 Q. Yao, M. Zhu, Z. Yang, X. Song, X. Yuan, Z. Zhang, W. Hu and J. Xie, *Nat. Rev. Mater.*, 2025, **10**, 89–108.
59 M. F. Matus and H. Häkkinen, *Nat. Rev. Mater.*, 2023, **8**, 372–389.
60 (*a*) Z. Li, Y. Li, Y. Liu, K. Li, F. Fu, M. Liu, J. Yuan, T. Zhang, J. Wang, Y. Li, F. Shen, H. Liu, P. Wang and D. Liu, CCDC 2403377: Experimental Crystal Structure Determination, 2025, DOI: **10.5517/ccdc.csd.cc2lnx9h**; (*b*) Z. Li, Y. Li, Y. Liu, K. Li, F. Fu, M. Liu, J. Yuan, T. Zhang, J. Wang, Y. Li, F. Shen, H. Liu, P. Wang and D. Liu, CCDC 2403378: Experimental Crystal Structure Determination, 2025, DOI: **10.5517/ccdc.csd.cc2lnxbj**.